

Singular limit analysis of a model for earthquake faulting

**Elena Bossolini, Morten Brøns and Kristian Uldall
Kristiansen**

Department of Applied Mathematics and Computer Science, Technical University of Denmark, Kongens Lyngby 2800, DK

E-mail: ebos@dtu.dk, mobr@dtu.dk, krkri@dtu.dk

Abstract. In this paper we consider a one dimensional spring-block model describing earthquake faulting. By using geometric singular perturbation theory and the blow-up method we provide a detailed description of the periodicity of the earthquake episodes. In particular we show that the limit cycles arise from a degenerate Hopf bifurcation whose degeneracy is due to an underlying Hamiltonian structure that leads to large amplitude oscillations. We use a Poincaré compactification to study the system near infinity. At infinity the critical manifold loses hyperbolicity with an exponential rate. We use an adaptation of the blow-up method to recover the hyperbolicity. This enables the identification of a new attracting manifold that organises the dynamics at infinity. This in turn leads to the formulation of a conjecture on the behaviour of the limit cycles as the time-scale separation increases. We illustrate our findings with numerics and suggest an outline of the proof of this conjecture.

PACS numbers:

Keywords: singular perturbation; Hamiltonian systems; rate and state friction; blow-up; earthquake dynamics; Poincaré compactification

Submitted to: *Nonlinearity*

1. Introduction

Earthquake events are a non-linear multi-scale phenomenon. Some of the non-linear occurrences are fracture healing, repeating behaviour and memory effects (Ruina 1983, Heaton 1990, Vidale et al. 1994, Marone 1998*b*). In this paper we focus on the repeating behaviour of the earthquake cycles, where a cycle is defined as the combination of a rupture event with a following healing phase. An earthquake rupture consists of the instantaneous slipping of a fault side relative to the other side. The healing phase allows the fault to strengthen again and this process evolves on a longer time scale than the rupture event (Carlson & Langer 1989, Marone 1998*a*).

The repetition of the earthquake events is significant for the predictability of earthquake hazards. The data collected in the Parkfield experiment in California show evidence of recurring micro-earthquakes (Nadeau & McEvilly 1999, Marone et al. 1995, Bizzarri 2010, Zechar & Nadeau 2012). For large earthquakes it is harder to detect a repeating pattern from the data, even though recent works indicate the presence of recurring cycles (Ben-Zion 2008).

The one dimensional spring-block model together with the empirical Ruina friction law is a fundamental model to describe earthquake dynamics (Burrige & Knopoff 1967, Ruina 1983, Rice & Ruina 1983, Gu et al. 1984, Rice & Tse 1986, Carlson et al. 1991, Belardinelli & Belardinelli 1996, Fan et al. 2014). Although the model does not represent all the non-linear phenomena of an earthquake rupture, it still reproduces the essential properties of the fault dynamics as extrapolated from experiments on rocks. The dimensionless form of the model is:

$$\begin{aligned} \dot{x} &= -e^z (x + (1 + \alpha)z), \\ \dot{y} &= e^z - 1, \\ \varepsilon \dot{z} &= -e^{-z} \left(y + \frac{x + z}{\xi} \right). \end{aligned} \tag{1}$$

Numerically, it has been observed that (1) has periodic solutions corresponding to the recurrence of the earthquake episodes, as shown in Figure 1 for two different values of the parameter ε and $\alpha > \xi$ fixed. The steep growth of the y -coordinate corresponds to the earthquake rupture, while the slow decay corresponds to the healing phase. Hence the periodic solutions of (1) have a multiple time-scale dynamics. Furthermore in Figure 1 we observe that the amplitude of the oscillations increases for decreasing values of the time-scale separation ε . For these reasons

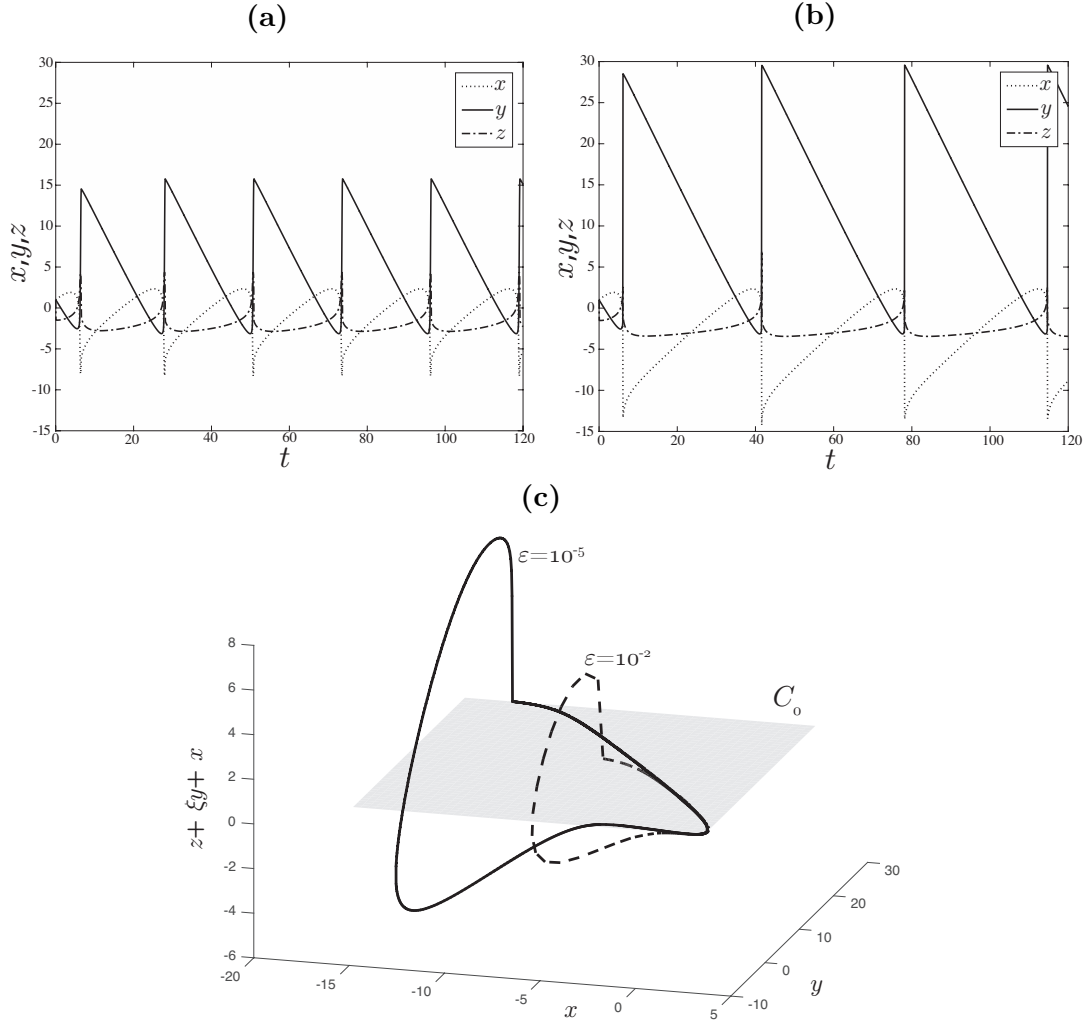


Figure 1: Numerical simulations of (1) for $\alpha = 0.9$ and $\xi = 0.5$. $\epsilon = 10^{-2}$ in (a) while $\epsilon = 10^{-5}$ in (b). In (c) phase space of both simulations. The grey plane C_0 and the coordinate $z + \xi y + x$ are clarified in section 3.

extensive numerical simulations are difficult to perform in the relevant parameter range, that is $\epsilon \in [10^{-24}, 10^{-8}]$ (Rice & Tse 1986, Carlson & Langer 1989, Madariaga & Cochard 1996, Lapusta et al. 2000, Erickson et al. 2008, Erickson et al. 2011). We remark that the periodic solutions of (1) appear in a finite interval of values of $\alpha > \xi$. If α is much larger than ξ then chaotic dynamics emerges, as documented by Erickson et al. (2008).

It is the purpose of the present paper to initiate a rigorous mathematical study of (1) as a singular perturbation problem (Jones 1995, Kaper 1999). At the singular limit $\varepsilon = 0$ we find an unbounded *singular cycle* when $\alpha > \xi$. For $\varepsilon > 0$ we conjecture this cycle to perturb into a stable, finite amplitude limit cycle that explains the behaviour of Figure 1. In this way we can predict the periodic solutions of (1) even in parameter regions that are not possible to explore numerically. We expect that the deeper understanding of (1) that we provide, together with the techniques that we introduce, can be of help to study the continuum formulation of the Burridge and Knopoff model, in particular regarding the analysis of the Heaton pulses (Heaton 1990).

As we will see in section 3, in our analysis the critical manifold loses normal hyperbolicity at infinity with an exponential rate. This is a non-standard loss of hyperbolicity that also appears in other problems (Rankin et al. 2011). To deal with this issue we will first introduce a compactification of the phase space with the Poincaré sphere (Chicone 2006) and repeatedly use the blow-up method of Dumortier & Roussarie (1996) in the version of Krupa & Szmolyan (2001). In particular we will use a technique that has been recently analyzed in (Kristiansen 2016). For an introduction to the blow-up method we refer to (Kuehn 2015).

Another way to study system (1) when $\varepsilon \ll 1$ is by using the method of matched asymptotic expansions, see (Eckhaus 1973) for an introduction. Putelat et al. (2008) have done the matching of the different time scales of (1) with an energy conservation argument, while in (Pomeau & Berre 2011) the causes of the switch between the two different time scales are not studied. However, the relaxation oscillation behavior of the periodic solutions of (1) is not explained.

Our paper is structured as follows. In section 2 we briefly discuss the physics of system (1). In section 3 we set (1) in the formalism of geometric singular perturbation theory and in section 4 we consider the analysis of the reduced problem for $\alpha = \xi$ and $\varepsilon = 0$. Here a degenerate Hopf bifurcation appears whose degeneracy is due to an underlying Hamiltonian structure that we identify. We derive a bifurcation diagram in section 5 after having introduced a compactification of the reduced problem. From this and from the analysis of section 6, we conclude that the limit cycles of Figure 1 cannot be described by the sole analysis of the reduced problem. In section 7 we define a candidate *singular cycle* Γ_0 that is used in our main result, Conjecture 7.1. This conjecture is on the existence of limit cycles $\Gamma_\varepsilon \rightarrow \Gamma_0$ for $\varepsilon \ll 1$. The conjecture is supported by numerical simulations but in sections 8 and 9 we also lay out the foundation of a proof by using the blow-up method to gain hyperbolicity of

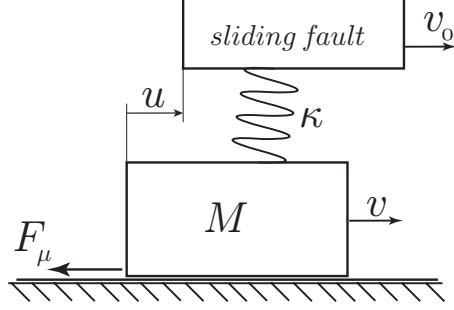


Figure 2: Spring-block model describing the earthquake faulting.

Γ_0 . Finally in section 10 we conclude and summarize the results of our analysis.

2. Model

The one dimensional spring-block model is presented in Figure 2. We suppose that one fault side slides at a constant velocity v_0 and drags the other fault side of mass M through a spring of stiffness κ . The friction force $F_\mu = \sigma\mu$ acts against the motion. A common assumption is to suppose that the normal stress σ , i.e. the stress normal to the friction interface (Nakatani 2001), is constant $\sigma = 1$. The friction coefficient μ is modelled with the Ruina rate and state friction law $\mu = \mu(v, \theta)$, with v the sliding velocity and θ the *state* variable. The state θ accounts for how long the two surfaces have been in contact (Ruina 1983, Marone 1998b). The equations of our model are:

$$\begin{aligned}\theta' &= -\frac{v}{L} \left(\theta + b \ln \left(\frac{v}{v_0} \right) \right), \\ u' &= v - v_0, \\ Mv' &= -\kappa u - \left(\theta + a \ln \left(\frac{v}{v_0} \right) \right),\end{aligned}\tag{2}$$

where the variable u is the relative displacement between the two fault sides and the prime denotes the time derivative. The parameter L is the characteristic displacement that is needed to recover the contact between the two surfaces when the slip occurs, while a and b are empirical coefficients that depend on the material properties (Marone 1998b). We introduce the dimensionless coordinates (x, y, w, t)

into system (2), where $\theta = ax$, $u = Ly$, $v = v_0w$, $t = (v_0/L)t'$:

$$\begin{aligned}\dot{x} &= -w(x + (1 + \alpha)\ln(w)), \\ \dot{y} &= w - 1, \\ \varepsilon\dot{w} &= -y - \frac{x + \ln(w)}{\xi}.\end{aligned}\tag{3}$$

We notice that equation (3) has a singularity in $w = 0$ and to avoid it we henceforth introduce the variable $z = \ln(w)$ so that we obtain the formulation presented in (1). In system (3) we have introduced the parameters: $\varepsilon = Mv_0^2/(\kappa L^2)$ such that $1/\sqrt{\varepsilon}$ is a non-dimensional frequency, $\xi = (\kappa L)/a$: the non-dimensional spring constant and $\alpha = (b - a)/b$ describing the sensitivity to the velocity relaxation (Erickson et al. 2008). We consider the parameter values presented by Madariaga (1998): $\varepsilon \in [10^{-24}, 10^{-8}]$, $\xi = 0.5$, $\alpha > \xi$. An extensive reference to the parameter sets is in the work of Dieterich (1972, 1978, 1979). We choose to keep the parameter $\xi > 0$ fixed (selecting $\xi = 0.5$ in our computations) and we use α as the bifurcation parameter. With this choice the study of (1) as a singular perturbation problem is simplified. Indeed as we will see in section 3, the critical manifold of (1) is a surface that depends on ξ . The results of our analysis can be easily interpreted for the case of α fixed and ξ varying, that is the standard approach in the literature.

3. Singular perturbation approach to the model

The positive constant $\varepsilon \ll 1$ in system (1) measures the separation of two time scales. In particular the variables (x, y) are slow while z is fast. We call equation (1) the slow problem and the dot refers to the differentiation with respect to the slow time t . We introduce the fast time $\tau = t/\varepsilon$ to obtain the fast problem:

$$\begin{aligned}x' &= -\varepsilon e^z(x + (1 + \alpha)z), \\ y' &= \varepsilon(e^z - 1), \\ z' &= -e^{-z}\left(y + \frac{x + z}{\xi}\right),\end{aligned}\tag{4}$$

where the prime stands for differentiation with respect to τ . The two systems (1) and (4) are equivalent whenever $\varepsilon > 0$. In the singular analysis we consider two

different limit systems. By setting $\varepsilon = 0$ in (1) we obtain the reduced problem:

$$\begin{aligned} \dot{x} &= -e^z(x + (1 + \alpha)z), \\ \dot{y} &= e^z - 1, \\ 0 &= -e^{-z} \left(y + \frac{x + z}{\xi} \right), \end{aligned} \tag{5}$$

that is also referred in the literature as the quasi-static slip motion (specifically $M \rightarrow 0$ in (2), (Ruina 1983)). Setting $\varepsilon = 0$ in (4) gives the layer problem:

$$z' = -e^{-z} \left(y + \frac{x + z}{\xi} \right), \quad (x, y)(\tau) = (x^0, y^0). \tag{6}$$

System (6) has a plane of fixed points that we denote the critical manifold:

$$C_0 := \left\{ (x, y, z) \in \mathbb{R}^3 \mid z = -x - \xi y \right\}. \tag{7}$$

This manifold, depicted in grey in Figure 1(c), is attracting:

$$\left. \frac{\partial z'}{\partial z} \right|_{C_0} = -\xi^{-1} e^{-z} < 0. \tag{8}$$

The results by Fenichel (1974, 1979) guarantee that close to C_0 there is an attracting (due to (8)) slow-manifold S_ε for any compact set $(x, y) \in \mathbb{R}^2$ and ε sufficiently small. However we notice in (8) that C_0 loses its normal hyperbolicity at an exponential rate when $z \rightarrow +\infty$. This is a key complication: orbits leave a neighborhood of the critical manifold even if it is formally attracting. This is a non-standard loss of hyperbolicity that appears also in other physical problems (Rankin et al. 2011). To our knowledge, (Kristiansen 2016) is the first attempt on a theory of exponential loss of hyperbolicity. In section 8 we will apply the method described in (Kristiansen 2016) to resolve the loss of hyperbolicity at infinity. In this paper we do not aim to give a general geometric framework to this approach. In the case of loss of hyperbolicity at an algebraic rate, like in the autocatalator problem studied originally by Gucwa & Szmolyan (2009), we refer to the work of Kuehn (2014).

Naïvely we notice that when $z \gg 1$ the dynamics of system (1) is driven by a new time scale, that is not related to its slow-fast structure. Assuming $z \gg \ln \varepsilon^{-1}$ we can rewrite (1) as:

$$\begin{aligned} \dot{x} &= -x - (1 + \alpha)z, \\ \dot{y} &= 1, \\ \dot{z} &= 0, \end{aligned} \tag{9}$$

where we have further rescaled the time by dividing the right hand side by e^z and ignored the higher order terms. Hence in this regime there is a family of x -nullclines:

$$x + (1 + \alpha)z = 0, \quad (10)$$

that are attracting since:

$$\frac{\partial \dot{x}}{\partial x} = -1.$$

This naïve approach is similar to the one used by Rice & Tse (1986) to describe the different time scales that appear in system (1).

4. Reduced Problem

We write the reduced problem (5) as a vector field $f_0(y, z; \alpha)$ by eliminating x in (5):

$$f_0(y, z; \alpha) := \begin{cases} \dot{y} &= e^z - 1, \\ \dot{z} &= \xi + e^z (\alpha z - \xi y - \xi). \end{cases} \quad (11)$$

The following proposition describes the degenerate Hopf bifurcation at the origin of (11) for $\alpha = \xi$.

Proposition 4.1 *The vector field (11) has a unique fixed point in $(y, z) = (0, 0)$ that undergoes a degenerate Hopf bifurcation for $\alpha = \xi$. In particular $f_0(y, z; \xi)$ is Hamiltonian and it can be rewritten as:*

$$f_0(y, z; \xi) = g(y, z)J\nabla H(y, z), \quad (12)$$

with

$$g(y, z) = \frac{e^{\xi y + z}}{\xi}, \quad (13a)$$

$$H(y, z) = -e^{-\xi y} (\xi y - \xi z + \xi + 1 - \xi e^{-z}) + 1, \quad (13b)$$

and where J is the standard symplectic structure matrix: $J = \begin{bmatrix} 0 & 1 \\ -1 & 0 \end{bmatrix}$.

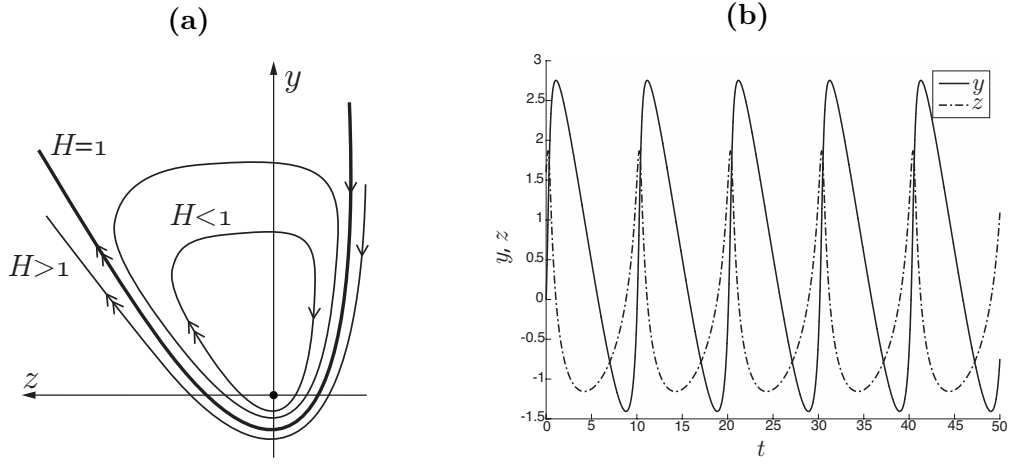


Figure 3: Behaviour of the reduced problem (12) for $\alpha = \xi$. In (a): phase space. The axis orientation is chosen in order to be consistent with the remaining figures of the paper. In (b): simulation of (12) for $H = 0.4$, $\xi = 0.5$.

Proof The linear stability analysis of (11) in the fixed point $(y, z) = (0, 0)$ gives the following Jacobian matrix:

$$Df_0(0, 0; \alpha) = \begin{bmatrix} 0 & 1 \\ -\xi & \alpha - \xi \end{bmatrix}. \quad (14)$$

The trace of (14) is zero for $\alpha = \xi$ and its determinant is $\xi > 0$. Hence a Hopf bifurcation occurs. The direct substitution of (13) into (12) shows that system (11) is Hamiltonian for $\alpha = \xi$. Therefore the Hopf bifurcation is degenerate. \square

The Hopf bifurcation of (11) for $\alpha = \xi$ is a known result (Ruina 1983, Putelat et al. 2008, Erickson et al. 2008). The function $H(y, z)$ has been used as a Lyapunov function in (Gu et al. 1984) without realising the Hamiltonian structure of (11).

From Proposition 4.1 we obtain a vertical family of periodic orbits for $\alpha = \xi$. The phase space of (12) is illustrated in Figure 3(a) for positive values of $H(y, z)$. We remark that the fixed point $(y, z) = (0, 0)$ is associated with $H(y, z) = 0$.

The intersection of the y -axis with the orbits $H(y, z) = h$ corresponds to the real roots of the Lambert equation:

$$-e^{-\xi y}(\xi y + 1) + 1 = h, \quad h \geq 0. \quad (15)$$

Equation (15) has a real root for any $h > 0$ in the region $y < 0$, while a second real root in the region $y > 0$ exists only for $h \in (0, 1)$ (Corless et al. 1996). The

intersection of the Hamiltonian trajectories with the y -axis is transversal for all $h > 0$, since the following condition holds:

$$\frac{\partial H}{\partial y}(y, 0) = \xi^2 y e^{-\xi y} \neq 0, \quad \forall y \neq 0. \quad (16)$$

The trajectory identified with $H(y, z) = 1$ (that is in bold in Figure 3(a)) plays a special role since it separates the closed orbits for $H \in (0, 1)$ from the unbounded ones for $H \geq 1$. Our analysis supports the results of Gu et al. (1984) and contrasts (Ranjith & Rice 1999) where it is claimed that (12) has no unbounded solutions.

Remark 1 *From (16) it follows that the function $H(y, 0)$ defines a diffeomorphism between the points on the positive y -axis and the corresponding values $h \in (0, 1)$.*

Figure 3(b) highlights that the reduced problem (12) has an intrinsic slow-fastness. Indeed the phase space of (12) is swept with different speeds depending on the region considered. This feature is represented in Figure 3(a), with the double arrow representing fast motion. In particular when $z > 0$ the trajectories are swept faster than for $z < 0$. This is due to the exponential function in (11). The fast sweep for $z > 0$ corresponds to the steep increase in the y coordinate of Figure 3(b). This fast dynamics for $z > 0$ resembles the slip that happens during an earthquake rupture, while the slow motion for $z < 0$ matches the healing phase, recall Figure 1. From this observation we tend to disagree with the notation used in the literature, that calls the reduced problem the quasi-static slip phase (Ruina 1983).

In order to describe the unbounded trajectories with $H(y, z) \geq 1$ for $y, z \rightarrow \infty$ and to extend the analysis to the case $\alpha \neq \xi$, we introduce a compactification of the reduced problem (11) and then we rewrite (11) on the Poincaré sphere.

5. Compactification of the reduced problem

We define the Poincaré sphere $\mathcal{S}^{2,+}$ as:

$$\mathcal{S}^{2,+} := \{(Y, Z, W) \in \mathbb{R}^3 \mid Y^2 + Z^2 + W^2 = 1, \quad W \geq 0\}, \quad (17)$$

which projects the phase space of (11) onto the northern hemisphere of $\mathcal{S}^{2,+}$. We refer to (Chicone 2006) for further details on the compactification of vector fields. Geometrically (17) corresponds to embedding (11) into the plane $W = 1$ that we call the directional chart k_2 :

$$k_2 := \mathcal{S}^{2,+} \cap \{W = 1\}, \quad y_2 = \frac{Y}{W}, \quad z_2 = \frac{Z}{W},$$

and the dynamics on chart k_2 follows directly from (11) by variable substitution:

$$\begin{aligned} \dot{y}_2 &= e^{z_2} - 1, \\ \dot{z}_2 &= \xi + e^{z_2} (\alpha z_2 - \xi y_2 - \xi). \end{aligned} \tag{18}$$

The points at infinity in k_2 correspond to the condition $W = 0$, that is the equator of $\mathcal{S}^{2,+}$. To study the dynamics on the equator we introduce the two additional directional charts:

$$k_3 := \mathcal{S}^{2,+} \cap \{Z = 1\}, \quad y_3 = \frac{Y}{Z}, w_3 = \frac{W}{Z}, \tag{19a}$$

$$k_1 := \mathcal{S}^{2,+} \cap \{Y = 1\}, \quad z_1 = \frac{Z}{Y}, w_1 = \frac{W}{Y}. \tag{19b}$$

We follow the standard convention of Krupa & Szmolyan (2001) and use the subscript $i = 1, 2, 3$ to denote a quantity in chart k_i . We denote with k_{ij} the transformation from chart k_i to chart k_j for $i, j = 1, 2, 3$. We have the following change of coordinates:

$$k_{23} : \quad w_3 = z_2^{-1}, \quad y_3 = y_2 z_2^{-1}, \tag{20a}$$

$$k_{21} : \quad w_1 = y_2^{-1}, \quad z_1 = z_2 y_2^{-1}, \tag{20b}$$

$$k_{31} : \quad w_1 = w_3 y_3^{-1}, \quad z_1 = y_3^{-1}, \tag{20c}$$

that are defined for $z_2 > 0$, $y_2 > 0$ and $y_3 > 0$ respectively. The inverse transformations $k_{ji} = k_{ij}^{-1}$ are defined similarly. Figure 4 shows a graphical representation of the sphere and the directional charts.

We define $C_{0,\infty}$ as the extension of the critical manifold C_0 onto the equator of the sphere. From (8) it follows that $C_{0,\infty}$ is non-hyperbolic.

Proposition 5.1 *There exists a time transformation that is smooth for $W > 0$ and that de-singularizes the dynamics within $W = 0$, so that the reduced problem (11) has four fixed points $Q^{1,3,6,7}$ on $C_{0,\infty}$ satisfying:*

- Q^1 is an improper stable node with a single eigenvector tangent to $C_{0,\infty}$.
- Q^3 has one unstable direction that is tangent to $C_{0,\infty}$ and a unique center-stable manifold $W^{c,s}$.
- Q^6 has one stable direction that is tangent to $C_{0,\infty}$ and a unique center-unstable manifold $W^{c,u}$.

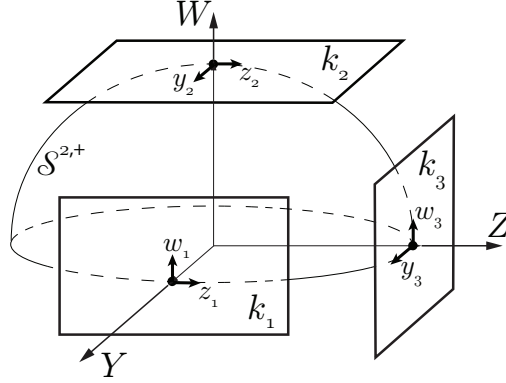


Figure 4: Poincaré sphere $\mathcal{S}^{2,+}$ and the directional charts $k_{1,2,3}$.

- Q^7 is an improper unstable node with a single eigenvector tangent to $C_{0,\infty}$.

The stability properties of the fixed points are independent of α , in particular both $W^{c,s}$ and $W^{c,u}$ are smooth in α .

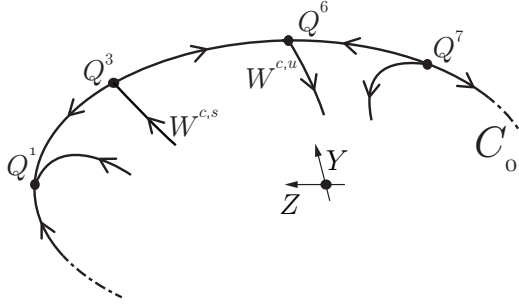


Figure 5: Fixed points on the compactified critical manifold C_0 .

Figure 5 gives a representation of the statements of Proposition 5.1. We remark that we use superscripts as enumeration of the points Q^m , $m = 1, 3, 6, 7$ to avoid confusion with the subscripts that we have used to define the charts k_i , $i = 1, 2, 3$. In particular the enumeration choice of the superscripts will become clear in section 7, where we will introduce the remaining points $Q^{2,4,5}$ in (53). In Proposition 5.2 we relate the structure at infinity of (11) to the dynamics on C_0 with respect to the parameter α .

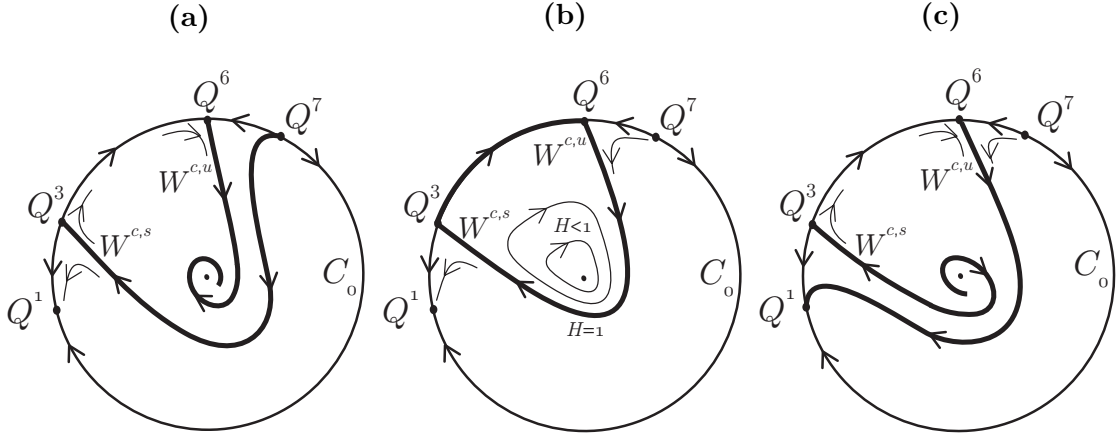


Figure 6: Bifurcation diagram of (11) with respect to the parameter α . Orbits spiral inwards for $\alpha < \xi$ (a) or outwards for $\alpha > \xi$ (c). In (b): $\alpha = \xi$.

Proposition 5.2 Fix $c > 0$ small and consider the parameter interval:

$$\alpha \in [\xi - c, \xi + c]. \quad (21)$$

Then Figure 6 describes the phase space of (11) with respect to α . In particular:

- When $\alpha < \xi$ the set $W^{c,s}$ separates the basin of attraction of $(y, z) = (0, 0)$ from the solutions that are forward asymptotic to Q^1 .
- When $\alpha = \xi$ Proposition 4.1 holds. The set $H = 1$ corresponds to $W^{c,s} \cap W^{c,u}$.
- When $\alpha > \xi$ the set $W^{c,u}$ separates the solutions that are backwards asymptotic to the origin to the ones that are backwards asymptotic to Q^7 .

Therefore no limit cycles appear in the reduced problem for $\varepsilon = 0$ and $\alpha \neq \xi$.

Remark 2 The local stability analysis of $(y, z) = (0, 0)$ can be directly obtained using $H(y, z)$ as a Lyapunov function. This was done in (Gu et al. 1984).

In the rest of the section we prove the previous two propositions. In sections 5.1 and 5.2 we perform an analysis of (11) in the two charts k_3 and k_1 respectively to show Proposition 5.1. We prove Proposition 5.2 in section 5.3.

5.1. Chart k_3

We insert (19a) into the reduced problem (18) and obtain the following system:

$$\begin{aligned}\dot{w}_3 &= -w_3(\alpha - \xi y_3) + \xi w_3^2(1 - e^{-\frac{1}{w_3}}), \\ \dot{y}_3 &= -y_3(\alpha - \xi y_3) - w_3(1 + \xi y_3)(1 - e^{-\frac{1}{w_3}}),\end{aligned}\tag{22}$$

here we have divided the right hand side by $\exp(1/w_3)$ to de-singularize $w_3 = 0$.

Remark 3 *The division by $\exp(1/w_3)$ in (22) is formally performed by introducing the new time t_3 such that:*

$$dt_3 = \exp(1/w_3)dt.\tag{23}$$

A similar de-singularization procedure is also used in the blow-up method.

System (22) has two fixed points:

$$Q^1 := (w_3, y_3) = (0, 0),\tag{24a}$$

$$Q^3 := (w_3, y_3) = \left(0, \frac{\alpha}{\xi}\right).\tag{24b}$$

The point Q^1 is a stable improper node with the double eigenvalue $-\alpha$ and a single eigenvector $(0, 1)^T$. The point Q^3 has one unstable direction $(0, 1)^T$ due to the positive eigenvalue α and a center direction $(\alpha/(1 + \alpha), 1)^T$ due to a zero eigenvalue. Notice that for $\alpha = \xi$ then $Q^3 = (0, 1)$.

Lemma 5.3 *There exists a unique center-stable manifold $W^{c,s}$ at the point Q^3 . This manifold is smooth in α . For $\alpha = \xi$ the set $H = 1$ coincides with $W^{c,s}$.*

Proof For $\alpha = \xi$ we rewrite the Hamiltonian (13b) in chart k_3 and insert the condition $H = 1$ to obtain the implicit equation:

$$\xi(y_3 - 1) + w_3(\xi + 1) - \xi w_3 e^{-\frac{1}{w_3}} = 0,\tag{25}$$

then $w_3 \rightarrow 0$ gives $y_3 \rightarrow 1$ that is the point Q^3 . As a consequence Q^3 has a saddle-like behaviour with an unique center-stable manifold $W^{c,s}$ tangent to $(\alpha/(1 + \alpha), 1)^T$. This invariant manifold $W^{c,s}$ is smooth in α and therefore it preserves its features for small variations of α from $\alpha = \xi$. \square

Remark 4 *With respect to t_3 the points within $W^{c,s}$ decay algebraically to Q^3 , while the decay towards the stable node Q^1 is exponential. Using (23) it then follows that all these points reach $w_3 = 0$ in finite time with respect to the original slow time t . This is a formal proof of the finite time blow-up of solutions of (11) for $\alpha > \xi$ that was also observed by Gu et al. (1984) and by Pomeau & Berre (2011).*

5.2. Chart k_1

We insert (19b) into the reduced problem (18) to obtain the dynamics in chart k_1 :

$$\begin{aligned}\dot{w} &= w^2(1 - e^{\frac{z}{w}}), \\ \dot{z} &= w(\xi + z)(1 - e^{\frac{z}{w}}) + e^{\frac{z}{w}}(\alpha z - \xi),\end{aligned}\tag{26}$$

where we have dropped the subscript for the sake of readability. We observe that the exponential term in (26) is not well defined in the origin. For this reason we introduce the blow-up transformation:

$$w = \bar{r}\bar{w}, \quad z = \bar{r}\bar{\zeta},\tag{27}$$

where $(\bar{w}, \bar{\zeta}) \in S^1 = \{(\bar{w}, \bar{\zeta}) : \bar{w}^2 + \bar{\zeta}^2 = 1\}$ and $\bar{r} \geq 0$. We consider the following charts:

$$\kappa_1 : \quad w = r_1\omega_1, \quad z = r_1,\tag{28a}$$

$$\kappa_2 : \quad w = r_2, \quad z = r_2\zeta_2,\tag{28b}$$

$$\kappa_3 : \quad w = r_3\omega_3, \quad z = -r_3.\tag{28c}$$

Next we perform an analysis of the blown-up vector field and the main results are summarized in Figure 7.

Chart κ_1 We insert condition (28a) into system (26) and divide the right hand side by $\exp(1/\omega_1)/r_1$ to get the de-singularized dynamics in chart κ_1 :

$$\begin{aligned}\dot{\omega}_1 &= \omega_1(\xi - \alpha r_1) + r_1\omega_1^2\xi \left(1 - e^{-\frac{1}{\omega_1}}\right), \\ \dot{r}_1 &= -r_1(\xi - \alpha r_1) - r_1^2\omega_1(\xi + r_1) \left(1 - e^{-\frac{1}{\omega_1}}\right).\end{aligned}\tag{29}$$

System (29) has one fixed point in $(\omega_1, r_1) = (0, \xi/\alpha)$ that corresponds to the point Q^3 introduced in (24b). Furthermore system (29) has a second fixed point

in $O_1 := (\omega_1, r_1) = (0, 0)$ with eigenvalues ξ , $-\xi$ and corresponding eigenvectors $(1, 0)^T$ and $(0, 1)^T$. Both the eigendirections of O_1 are invariant and we denote by γ_1 the heteroclinic connection between Q^3 and O_1 along the r_1 -axis.

The initial condition $p_{1,\text{in}}$ on $W^{c,s}$ with $\omega_1 = \delta > 0$ is connected through the stable and the unstable manifolds of O_1 to the point $p_{1,\text{out}} := (\omega_1, r_1) = (\delta^{-1}, 0)$ as shown in Figure 7(a).

Chart κ_2 We insert the transformation (28b) into (26) and divide the right hand side by $\exp(\zeta_2)/r_2$ to obtain the de-singularized vector field. In this chart there are no fixed points, yet the line $r_2 = 0$ is invariant and ζ_2 decreases monotonically along it. The orbit entering from chart κ_1 has the initial condition $p_{2,\text{in}} := \kappa_{12}(p_{1,\text{out}}) = (\zeta_2, r_2) = (\delta, 0)$ that lies on the invariant line $r_2 = 0$. Thus from $p_{2,\text{in}}$ we continue to the point $p_{2,\text{out}} := (\zeta_2, r_2) = (-\delta^{-1}, 0)$, as shown in Figure 7(b).

Chart κ_3 We introduce condition (28c) into the vector field (26) and divide by w_3 to obtain the de-singularized dynamics in chart κ_3 :

$$\begin{aligned}\dot{\omega}_3 &= (\xi - r_3)(1 - e^{-\frac{1}{\omega_3}}) + r_3\omega_3(1 - e^{-\frac{1}{\omega_3}}) + \frac{e^{-\frac{1}{\omega_3}}}{r_3}(\alpha r_3 + \xi), \\ \dot{r}_3 &= -r_3(\xi - r_3)(1 - e^{-\frac{1}{\omega_3}}) - \frac{e^{-\frac{1}{\omega_3}}}{\omega_3}(\alpha r_3 + \xi).\end{aligned}\tag{30}$$

System (30) has an unstable improper node in:

$$Q^7 := (\omega_3, r_3) = (0, \xi),\tag{31}$$

with double eigenvalue ξ and single eigenvector $(1, 0)^T$. For $w_3 = r_3 = 0$ the quantity $e^{-1/\omega_3}/r_3$ in (30) is not well defined. We deal with this singularity by first multiplying the right hand side of the vector field by $r_3\omega_3$:

$$\begin{aligned}\dot{\omega}_3 &= r_3\omega_3(\xi - r_3)(1 - e^{-\frac{1}{\omega_3}}) + r_3^2\omega_3^2(1 - e^{-\frac{1}{\omega_3}}) + \omega_3e^{-\frac{1}{\omega_3}}(\alpha r_3 + \xi), \\ \dot{r}_3 &= -r_3^2\omega_3(\xi - r_3)(1 - e^{-\frac{1}{\omega_3}}) - r_3e^{-\frac{1}{\omega_3}}(\alpha r_3 + \xi).\end{aligned}\tag{32}$$

Next we introduce the blow-up transformation:

$$\omega_3 = \rho, \quad r_3 = \frac{e^{-1/\rho}}{\rho}\eta.\tag{33}$$

We substitute (33) into (32) and we divide by $\exp(-1/\rho)/\rho$ to obtain the desingularized vector field:

$$\begin{aligned}\dot{\rho} &= \xi\rho^2(\eta - 1) + \mathcal{O}\left(\frac{\eta}{\rho}e^{-1/\rho}\right), \\ \dot{\eta} &= -\eta\xi(\eta - 1) + \mathcal{O}\left(\frac{\eta}{\rho}e^{-1/\rho}\right).\end{aligned}\tag{34}$$

Remark 5 *The blow-up map (33) is non-standard, since it is not written as an algebraic expression in ρ . To the author's knowledge there is no former literature treating blow-ups of the form (33) and in particular the approach of (Kristiansen 2016) does not treat this type of blow-ups.*

System (34) has two fixed points. The first fixed point $O_3 := (\rho, \eta) = (0, 0)$ has one unstable direction $(0, 1)^T$ associated with the eigenvalue ξ and one center direction $(1, 0)^T$ associated with the zero eigenvalue. The second fixed point is:

$$Q^6 := (\rho, \eta) = (0, 1),\tag{35}$$

and it has one stable direction $(0, 1)^T$ associated with the eigenvalue $-\xi$ and one center direction $(1, 0)^T$ associated with the zero eigenvalue. The axis $\rho = 0$ is invariant, thus there exists an heteroclinic connection along the η -axis between the points O_3 and Q^6 that we denote by γ_3 , see Figure 7(c).

Lemma 5.4 *There exists a unique center-unstable manifold $W^{c,u}$ at the point Q^6 that is smooth in α and that contains solutions that decay algebraically to Q^6 backwards in time. For $\alpha = \xi$ the set $H = 1$ coincides with $W^{c,u}$.*

Proof We rewrite the Hamiltonian (13b) in the (ρ, η) coordinates and then insert the condition $H = 1$ to obtain the implicit equation:

$$\frac{1}{\eta} - 1 + e^{-\frac{1}{\rho}} \left(\frac{1}{\rho} + 1 + \frac{1}{\xi} \right) = 0.\tag{36}$$

Here $\rho \rightarrow 0$ gives $\eta \rightarrow 1$. Therefore Q^6 has a saddle-like behaviour with a unique center-unstable manifold $W^{c,u}$ that is tangent to $(1, 0)^T$ in Q^6 . The invariant manifold $W^{c,u}$ is smooth in α and it maintains the center-unstable properties for small variation of α from $\alpha = \xi$. \square

The orbit entering from chart κ_2 in the point $p_{3,\text{in}} := \kappa_{23}(p_{2,\text{out}}) = (\rho, \eta) = (\delta, 0)$ is connected through the stable and the unstable manifolds of O_3 to the point $p_{3,\text{out}}$ on $W^{c,u}$ with $\omega_3 = \delta$ as shown in Figure 7(c).

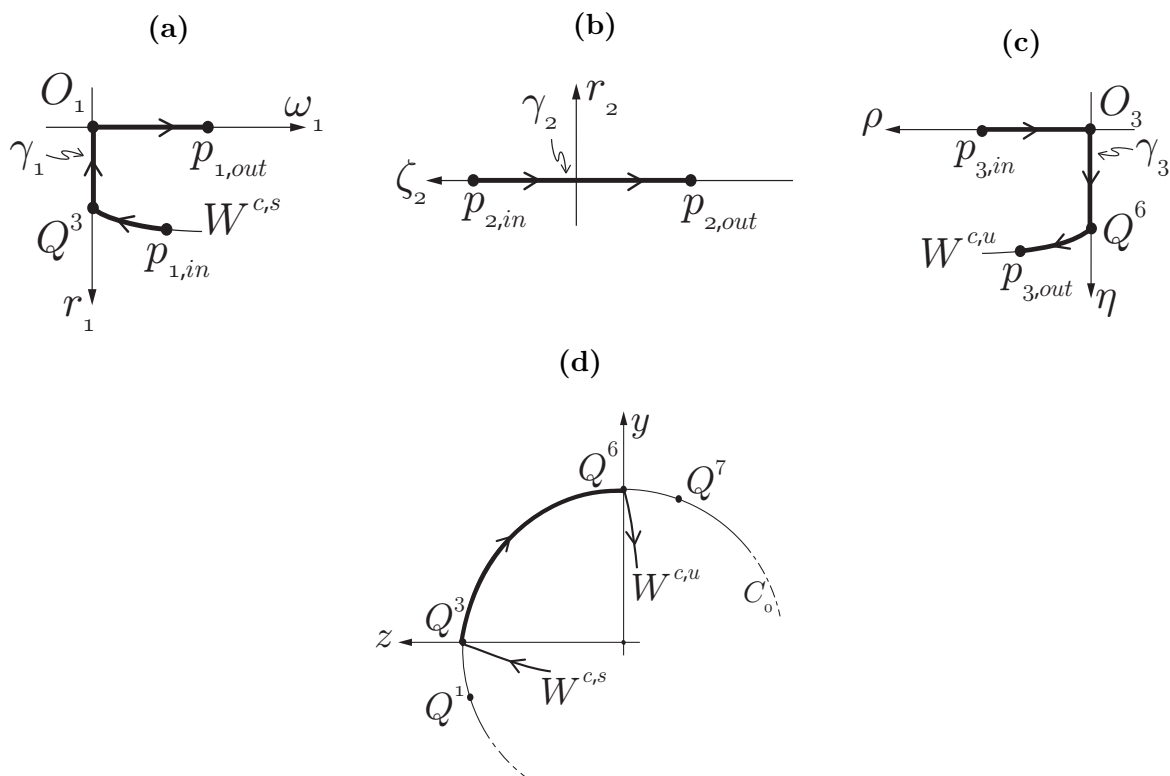


Figure 7: Blow-up of (26) in chart k_1 . (a), (b) and (c) represent charts κ_1, κ_2 and κ_3 respectively. In (d): behaviour at infinity after the blow-down.

Remark 6 We observe that the singularity at the origin of chart k_1 (26), upon blow-ups (27) and (33), has turned into three hyperbolic fixed points O_1, O_3 and Q^6 . After the blow-down we obtain the singular structure depicted in Figure 7(d).

5.3. The reduced problem on $\mathbb{S}^{2,+}$

The previous analysis has described the phase space of (11) near infinity. In the following we analyse the interaction of the unbounded solutions of the reduced problem (11) with the fixed points $Q^{1,3,6,7}$ for variations of the parameter α . We follow the Melnikov-type approach of Chow et al. (1994), to describe how the closed orbits of the Hamiltonian system (12) break up near $\alpha = \xi$.

When $\alpha = \xi$ any bounded trajectory of (12) with $H = h$, $h \in (0, 1)$, intersects the y -axis in the two points D, d that correspond to the two real roots of the Lambert

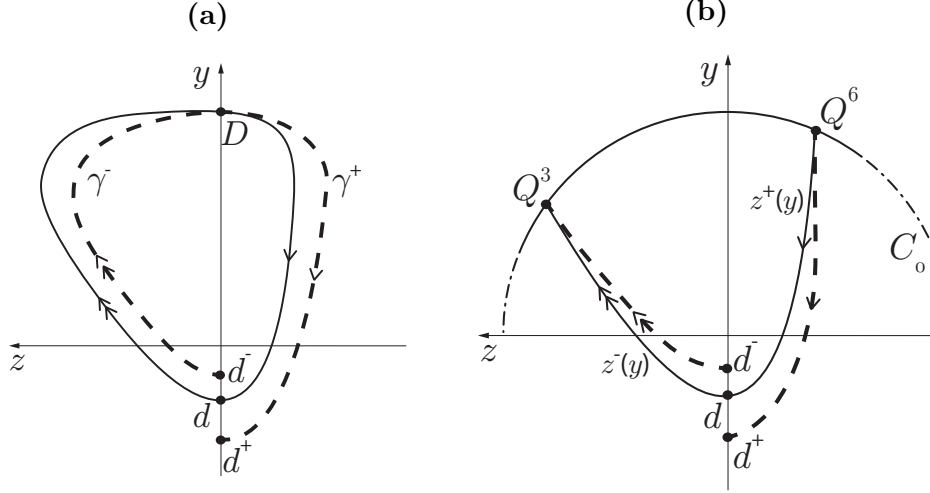


Figure 8: Perturbation of the Hamiltonian solutions for $\alpha - \xi$ small. In (a): closed orbit with $0 < H < 1$. In (b): heteroclinic connection for $H = 1$.

equation (15). We denote by D the root with $y > 0$ while we denote by d the one with $y < 0$, see Figure 8(a).

For $\alpha - \xi$ small, we compute the forward and backwards orbits $\gamma^+(t)$ and $\gamma^-(t)$ respectively emanating from D . The transversality condition (16) assures that $\gamma^+(t)$ and $\gamma^-(t)$ cross the y -axis for the first time in the points d^+ and d^- respectively. Hence we define the distance function:

$$\begin{aligned}
\Delta(\alpha) &= H(d^+) - H(d^-), \\
&= \int_0^{T^+} \dot{H}(\gamma^+(t)) dt + \int_{T^-}^0 \dot{H}(\gamma^-(t)) dt, \\
&= \int_0^{T^+} \nabla H(h) \cdot f_0(y, z; \alpha) dt + \int_{T^-}^0 \nabla H(h) \cdot f_0(y, z; \alpha) dt,
\end{aligned} \tag{37}$$

where $T^\pm = T^\pm(\alpha) \geq 0$ is the flow-time between D and d^+ and between D and d^- respectively. We Taylor expand (37) around $\alpha = \xi$:

$$\Delta(\alpha) = (\alpha - \xi)\Delta_\alpha(h) + O((\alpha - \xi)^2), \tag{38}$$

with the quantity $\Delta_\alpha(h)$ defined as:

$$\begin{aligned}\Delta_\alpha(h) &= \int_{T_h^-}^{T_h^+} \nabla H(h) \cdot \frac{\partial f_0}{\partial \alpha}(y, z; \xi) dt \\ &= \int_{T_h^-}^{T_h^+} \xi e^{-\xi y} z (e^z - 1) dt.\end{aligned}\tag{39}$$

In (39) we have denoted with $(y, z)(t)$ the solution of (12) for $H = h$ and $\alpha = \xi$. The times $T_h^\pm = T_h^\pm(\xi)$ are the forward and backwards times from D to d . The integrand of (39) is always positive for $z \neq 0$ and therefore $\Delta_\alpha(h)$ is positive for any $h \in (0, 1)$. We conclude from (38) that the forward flow $\gamma^+(t)$ spirals outwards for $\alpha > \xi$ while it spirals inwards for $\alpha < \xi$, in agreement with Figure 6.

We now extend the analysis above to the case of $H = 1$. In this case the points d^+ and d^- are the intersections of $W^{c,u}$ and $W^{c,s}$ with the y -axis respectively, see Figure 8(b). From the analysis above we know that $W^{c,s}$ and $W^{c,u}$ depend smoothly on α .

Lemma 5.5 *For $\alpha = \xi$ there is a unique heteroclinic connection between Q^3 and Q^6 on C_0 . This connection is through the manifolds $W^{c,s}$ and $W^{c,u}$ and it corresponds to the set $H = 1$ in (13b). This set can be written as the union of two graphs $z = z^\pm(y)$ (see Figure 8(b)) with $y \geq -1/\xi$ so that $z^-(y)$ ($z^+(y)$ resp.) approaches Q^3 (Q^6) as $z^- = O(y)$ ($z^+ = O(\ln(y))$) for $y \rightarrow \infty$.*

Proof We rewrite the trajectory $H = 1$ as the graphs $z = z^\pm(y)$ for $y \geq -1/\xi$. The behaviour in forward time follows by considering the point $p_{1,\text{in}}$ in condition (25) and blowing it down to the original variables (y, z) . Similarly for the behaviour in backwards time by considering $p_{3,\text{out}}$ in condition (36). \square

Figure 6(b) follows from Lemma 5.5. When $\alpha = \xi$ the manifolds $W^{c,s}$ and $W^{c,u}$ cross the y -axis in the point $d := (y, z) = (-1/\xi, 0)$. We define the distance function $\Delta(\alpha)$ as in (37), we Taylor expand it around $\alpha = \xi$ as in (38) and we define $\Delta_\alpha(1)$ as in (39). Since the integrand of (39) is positive for $H = 1$ we just need to show that the improper integral (39) exists. From the reduced problem (11) we observe that $\dot{y} = e^z - 1$, thus we rewrite (39) with respect to y as:

$$\Delta_\alpha(1) = \int_{-1/\xi}^{+\infty} \xi e^{-\xi y} z^-(y) dy - \int_{-1/\xi}^{+\infty} \xi e^{-\xi y} z^+(y) dy.\tag{40}$$

Recall from Lemma 5.5 that $z^-(y)$ is asymptotically linear in y for $y \rightarrow \infty$, while $z^+(y)$ decreases logarithmically with respect to y . The expression (40) therefore exists because of the exponential decay of the factor $\exp(-\xi y)$ and furthermore it is positive. We remark that $\Delta_\alpha(h)$ in (39) converges to $\Delta_\alpha(1)$ for $h \rightarrow 1$, since the orbit segment on $C_{0,\infty}$ does not give any contribution to (40).

Now we finish the proof of Proposition 5.2 by considering α as in (21). When $\alpha < \xi$ the set $W^{c,u}$ contracts to the origin, because $\Delta(\alpha) < 0$ in (38). Furthermore the set $W^{c,s}$ is backwards asymptotic to Q^7 and acts as a separator between the basin of attraction of the origin and the basin of attraction of Q^1 . A similar argument covers the case $\alpha > \xi$. This concludes the proof of Proposition 5.2 and justifies Figures 6(a) and 6(c). Therefore no periodic orbit exists on C_0 for $\alpha > \xi$ and $\varepsilon = 0$.

6. Analysis of the perturbed problem for $\varepsilon > 0$

Consider the original problem (1) and $0 < \mu < 1$ small but fixed. Then the compact manifold:

$$S_0 = \{(x, y, z) \in C_0 \mid 0 \leq H(y, z) \leq 1 - \mu\}, \quad (41)$$

is normally hyperbolic for $\varepsilon = 0$. Therefore Fenichel's theory guarantees that for ε sufficiently small there exists a locally invariant manifold S_ε that is $O(\varepsilon)$ -close to S_0 and is diffeomorphic to it. Moreover the flow on S_ε converges to the flow of the reduced problem (11) for $\varepsilon \rightarrow 0$. A computation shows that S_ε at first order is:

$$z = -(x + \xi y) + \varepsilon \xi e^{-2(x+\xi y)} (\alpha(x + \xi y) + \xi(y + 1) - \xi e^{x+\xi y}) + O(\varepsilon^2),$$

hence we have the following vector field $f_\varepsilon(y, z; \alpha, \varepsilon)$ on S_ε :

$$f_\varepsilon(y, z; \alpha, \varepsilon) := \begin{cases} \dot{y} &= e^z - 1 - \varepsilon \xi \chi e^{2z} + O(\varepsilon^2), \\ \dot{z} &= \chi - \varepsilon \xi \chi e^{2z} (\alpha z - \xi y + \alpha - \xi + 1) + O(\varepsilon^2), \end{cases} \quad (42)$$

with $\chi(y, z) = \alpha z e^z - \xi y e^z - \xi e^z + \xi$.

Proposition 6.1 *Consider the compact manifold S_0 defined in (41). Then S_0 perturbs to a locally invariant slow manifold S_ε for $0 < \varepsilon \ll 1$. On S_ε the origin of (42) undergoes a supercritical Hopf bifurcation for:*

$$\alpha = \alpha_H := \xi - \varepsilon \xi^2 + O(\varepsilon^2), \quad (43)$$

with a negative first Lyapunov coefficient:

$$a = -\frac{1}{8}\varepsilon\xi^3(1 + \xi) + \mathcal{O}(\varepsilon^2) < 0. \quad (44)$$

Therefore for $\alpha \in (\alpha_H, \alpha_H + c(\mu)\varepsilon)$ with $c(\mu)$ sufficiently small, there exists a family of locally unique attracting limit cycles with amplitude of order $\mathcal{O}\left(\sqrt{-(\alpha - \alpha_H)/a}\right)$.

The proof of Proposition 6.1 follows from straightforward computations. We remark that since (44) is proportional to ε , it follows that the results of Proposition 6.1 are valid only for a very small interval of α around α_H . We use the analysis of section 5.3 to extend the small limit cycles of Proposition 6.1 into larger ones.

Proposition 6.2 *Consider the slow manifold S_ε of Proposition 6.1. On S_ε there exists a family of closed periodic orbits for*

$$\alpha = \alpha_M(h) := \xi - \varepsilon \frac{\Delta_\varepsilon(h)}{\Delta_\alpha(h)} + \mathcal{O}(\varepsilon^2), \quad (45)$$

where $h \in [c_1(\mu), 1 - c_2(\mu)]$ with $(c_1, c_2)(\mu)$ small. The quantity $\Delta_\varepsilon(h)$ is defined as:

$$\Delta_\varepsilon(h) = \int_{T_h^-}^{T_h^+} \nabla H(h) \cdot \frac{\partial f_\varepsilon}{\partial \varepsilon}(y, z; \xi, 0) dt, \quad (46)$$

while $\Delta_\alpha(h) > 0$ was defined in (39).

Proof By Fenichel's theorem we know that the flow on S_ε converges to the flow of the reduced problem (11) for $\varepsilon \rightarrow 0$. Therefore we can define the distance function $\Delta(\alpha, \varepsilon)$ similarly to (37) whose Taylor expansion around $\alpha = \xi$ and $\varepsilon = 0$ is:

$$\Delta(\alpha, \varepsilon) = (\alpha - \xi)\Delta_\alpha(h) + \varepsilon\Delta_\varepsilon(h) + \mathcal{O}((\alpha - \xi + \varepsilon)^2), \quad (47)$$

with $\Delta_\alpha(h)$ and $\Delta_\varepsilon(h)$ defined in (39) and (46) respectively. The integrand of $\Delta_\alpha(h)$ is strictly positive for all $h \in (0, 1)$, therefore we can apply the implicit function theorem to (47) for $\Delta(\alpha, \varepsilon) = 0$ and obtain the result (45). \square

In Figure 9 we show a numerical computation of the leading order coefficient in (45) for an interval of energies $H = h \in (0, 0.6]$. No saddle-node bifurcations occur in this interval and hence the periodic orbits are all asymptotically stable. We expect a similar behaviour for larger values of h but we did not manage to compute this due

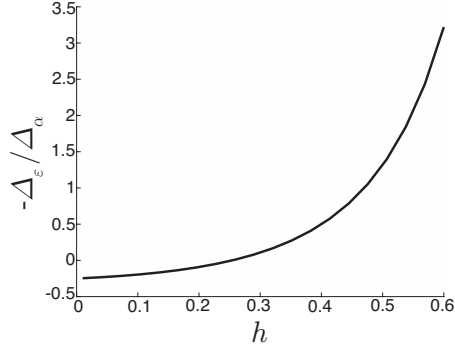


Figure 9: Plot of the leading order coefficient in (45) for $\xi = 0.5$ and $h \in (0, 0.6]$.

to the intrinsic slow-fast structure of the reduced problem. It might be possible to study the term $\Delta_\varepsilon(h)/\Delta_\alpha(h)$ analytically by using the results of Lemma 5.5 but the expressions are lengthy and we did not find an easy way.

The analysis above can only explain the limit cycles that appear for $\alpha - \xi = O(\varepsilon)$ and it does not justify the limit cycles of Figure 1 that appear for larger values of $\alpha - \xi$. For this reason we proceed to study the full problem (1) at infinity, introducing its compactification through the Poincaré sphere.

7. Statement of the main result

In this section we find a connection at infinity between the points Q^1 and Q^6 (recall Proposition 5.1) that will establish a return mechanism to C_0 of the unbounded solutions of (4) when $\varepsilon = 0$ and $\alpha > \xi$. This mechanism will be the foundation for the existence of limit cycles when $0 < \varepsilon \ll 1$ and $\alpha - \xi \geq c > 0$.

Similar to section 5, we introduce a four-dimensional Poincaré sphere $\mathcal{S}^{3,+}$:

$$\mathcal{S}^{3,+} := \{(X, Y, Z, W) \in \mathbb{R}^4 \mid X^2 + Y^2 + Z^2 + W^2 = 1, \quad W \geq 0\}. \quad (48)$$

The fast problem (4) is interpreted as a directional chart K_2 on $\mathcal{S}^{3,+}$ defined for $W = 1$:

$$K_2 := \mathcal{S}^{3,+} \cap \{W = 1\}, \quad x_2 = \frac{X}{W}, y_2 = \frac{Y}{W}, z_2 = \frac{Z}{W},$$

therefore the vector field in chart K_2 is obtained by introducing the subscript in (4):

$$\begin{aligned} \dot{x}_2 &= -\varepsilon e^{z_2}(x_2 + (1 + \alpha)z_2), \\ \dot{y}_2 &= \varepsilon (e^{z_2} - 1), \\ \dot{z}_2 &= -e^{-z_2} \left(y_2 + \frac{x_2 + z_2}{\xi} \right). \end{aligned} \tag{49}$$

The points at infinity in K_2 correspond to $W = 0$ which is a sphere S^2 . We introduce the two directional charts:

$$K_3 := \mathbb{S}^{3,+} \cap \{Z = 1\}, \quad x_3 = \frac{X}{Z}, y_3 = \frac{Y}{Z}, w_3 = \frac{W}{Z}, \tag{50a}$$

$$K_1 := \mathbb{S}^{3,+} \cap \{Y = 1\}, \quad x_1 = \frac{X}{Y}, z_1 = \frac{Z}{Y}, w_1 = \frac{W}{Y}. \tag{50b}$$

We have the following transformations between the charts:

$$K_{23} : \quad w_3 = z_2^{-1}, \quad x_3 = x_2 z_2^{-1}, \quad y_3 = y_2 z_2^{-1}, \tag{51a}$$

$$K_{21} : \quad w_1 = y_2^{-1}, \quad x_1 = x_2 y_2^{-1}, \quad z_1 = z_2 y_2^{-1}, \tag{51b}$$

$$K_{31} : \quad w_1 = w_3 y_3^{-1}, \quad x_1 = x_3 y_3^{-1}, \quad z_1 = y_3^{-1}, \tag{51c}$$

that are defined for $z_2 > 0$, $y_2 > 0$ and $y_3 > 0$ respectively. The inverse transformations are defined similarly. The three points $Q^1, Q^3 \in K_3$ and $Q^6 \in K_1$:

$$Q^1 := (x_3, y_3, w_3) = (-1, 0, 0), \tag{52a}$$

$$Q^3 := (x_3, y_3, w_3) = \left(-1 - \alpha, \frac{\alpha}{\xi}, 0 \right), \tag{52b}$$

$$Q^6 := (x_1, z_1, w_1) = (-\xi, 0, 0), \tag{52c}$$

introduced in Proposition 5.1 and the three points $Q^2, Q^4 \in K_3$ and $Q^5 \in K_1$:

$$Q^2 := (x_3, y_3, w_3) = (-1 - \alpha, 0, 0), \tag{53a}$$

$$Q^4 := (x_3, y_3, w_3) = \left(-1 - \alpha, \frac{2\alpha}{\xi}, 0 \right), \tag{53b}$$

$$Q^5 := (x_1, z_1, w_1) = \left(-\frac{\xi}{2\alpha}(1 + \alpha), \frac{\xi}{2\alpha}(1 - \alpha), 0 \right), \tag{53c}$$

are going to play a role in the following, together with the lines:

$$L_0 := \{(x_3, y_3, w_3) \mid x_3 + 1 + \alpha = 0, w_3 = 0\}, \quad (54a)$$

$$C_{0,\infty} := \{(x_3, y_3, w_3) \mid x_3 + \xi y_3 + 1 = 0, w_3 = 0\}. \quad (54b)$$

Notice that the line L_0 corresponds to the intersection of the family of nullclines (10) with infinity through K_{23} . We construct the following *singular cycle*:

Definition Let Γ_0 be the closed orbit consisting of the points $Q^{1,2,4,5,6}$ and of the union of the following sets:

- $\gamma^{1,2}$ connecting Q^1 with Q^2 . In chart K_3 the segment $\gamma^{1,2}$ is:

$$\gamma^{1,2} := \{(x_3, y_3, w_3) \in K_3 \mid x_3 \in (-1 - \alpha, -1), y_3 = 0, w_3 = 0\}. \quad (55)$$

- $\gamma^{2,4}$ connecting Q^2 with Q^4 along L_0 . In chart K_3 the segment $\gamma^{2,4}$ is:

$$\gamma^{2,4} := \left\{ (x_3, y_3, w_3) \in K_3 \mid x_3 = -1 - \alpha, y_3 \in \left(0, \frac{2\alpha}{\xi}\right), w_3 = 0 \right\}. \quad (56)$$

- $\gamma^{4,5}$ connecting Q^4 with Q^5 . This segment is a fast fiber of (6) and in chart K_1 the segment $\gamma^{4,5}$ is:

$$\gamma^{4,5} := \left\{ (x_1, z_1, w_1) \in K_1 \mid x_1 = -\frac{\xi}{2\alpha}(1 + \alpha), z_1 \in \left(\frac{\xi}{2\alpha}(1 - \alpha), \frac{\xi}{2\alpha}\right), w_1 = 0 \right\}. \quad (57)$$

- $\gamma^{5,6}$ connecting Q^5 with Q^6 on $C_{0,\infty}$. In chart K_1 the segment $\gamma^{5,6}$ is:

$$\gamma^{5,6} := \left\{ (x_1, z_1, w_1) \in K_1 \mid x_1 = -\xi - z_1, z_1 \in \left(0, \frac{\xi}{2\alpha}(1 - \alpha)\right), w_1 = 0 \right\}. \quad (58)$$

- $W^{c,u}$ connecting Q^6 with Q^1 on the critical manifold C_0 .

In section 8 we identify Γ_0 using repeatedly the blow-up method on system (49). Figure 10 shows Γ_0 and its different segments: 10(a) displays the complete cycle while 10(b) and 10(c) illustrate the portions of Γ_0 that are visible in the charts K_3 and K_1 respectively. Γ_0 plays an important role in our main result, since we conjecture it to be the candidate *singular cycle*:

Conjecture 7.1 *Fix $\alpha > \xi$. Then for $0 < \varepsilon \ll 1$ there exists an attracting limit cycle Γ_ε that converges to the singular cycle Γ_0 for $\varepsilon \rightarrow 0$.*

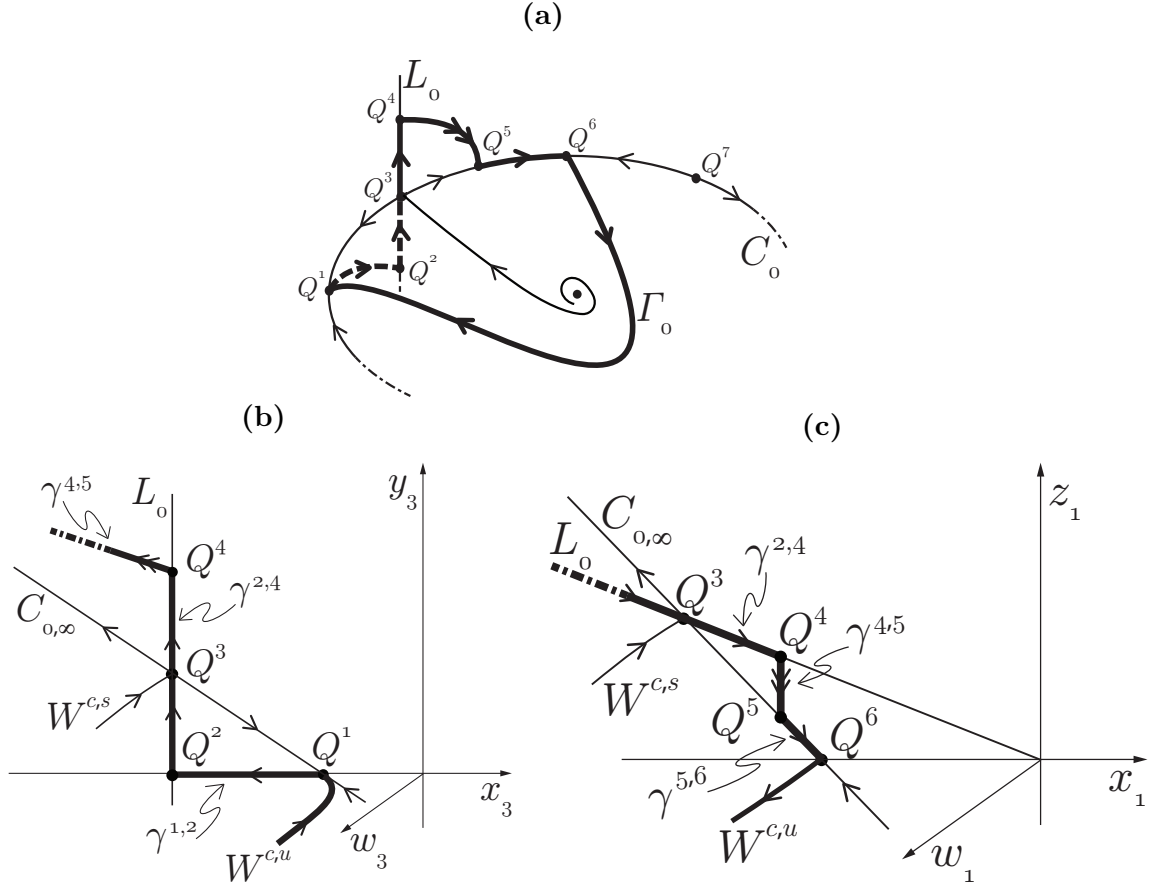


Figure 10: Schematisation of Γ_0 in (a). In chart K_3 (b) we see the segments $\gamma^{1,2}, \gamma^{2,4}$ and partially $\gamma^{4,5}$. In chart K_1 (c) we see $\gamma^{4,5}, \gamma^{5,6}$ and partially $\gamma^{2,4}$.

A rigorous proof of Conjecture 7.1 requires an analysis both for $\varepsilon = 0$ and $0 < \varepsilon \ll 1$. In section 9 we outline a procedure to prove the conjecture and we leave the full details of the proof to a future manuscript.

Remark 7 Here we collect the results of sections 6 and 7. When $\varepsilon = 0$ and $\alpha = \xi$ then there exists a family of periodic solutions on $\mathcal{S}^{3,+}$, corresponding to the Hamiltonian orbits with $H \in (0, 1)$. For $\alpha > \xi$ only the cycle Γ_0 persists.

When $0 < \varepsilon \ll 1$ and $\alpha - \xi = O(\varepsilon)$ there exists a limit cycle resembling the bounded Hamiltonian orbits. For larger values of $\alpha - \xi$ we conjecture that the limit cycle tends to Γ_0 . Figure 11 shows the conjectured bifurcation diagram of the periodic orbits.

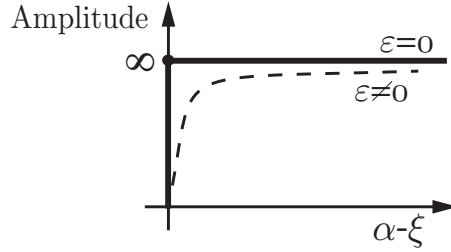


Figure 11: Conjectured bifurcation diagram of the limit cycles for $\varepsilon \ll 1$.

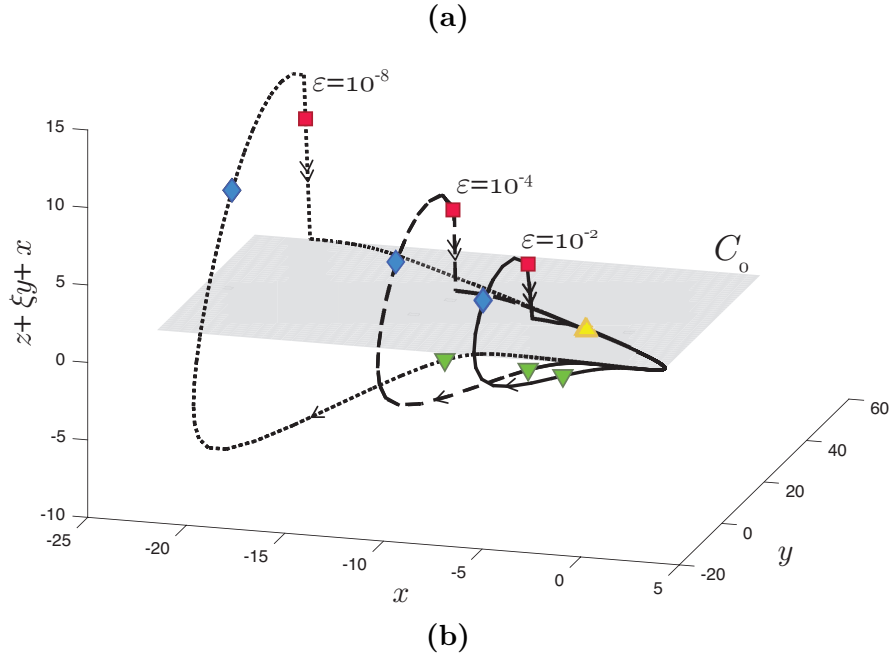
Figure 11 shows some numerical simulations supporting Conjecture 7.1: 12(a) illustrates the limit cycles Γ_ε for three different values of $\varepsilon \in \{10^{-8}, 10^{-4}, 10^{-2}\}$ with $\alpha = 0.9$ and $\xi = 0.5$ while 12(b) and 11(a) show the portions of Γ_ε that appear in the charts K_3 and K_1 respectively. The amplitudes of the orbits increase for decreasing values of the parameter ε and both the plane C_0 and the line L_0 play an important role. Close to the origin the dynamics evolves on C_0 while sufficiently far from the origin L_0 becomes relevant. Indeed in Figure 12(b) we see that the solutions contract to L_0 following $\gamma^{1,2}$ and then they evolve following $\gamma^{2,4}$. When the trajectories are close to Q^4 they follow $\gamma^{4,5}$ and contract again towards C_0 along a direction that tends to the fast fiber for $\varepsilon \rightarrow 0$, as we can see in Figure 11(a).

8. Identification of the segments of Γ_0 at infinity

In this section we focus on the identification of the segments of Γ_0 (55)–(58). We are especially interested in revealing the line L_0 and the segments that interact with it. In 8.1 we study the dynamics along chart K_3 and then in 8.2 we consider chart K_1 . More details are available in (Bossolini et al. 2016).

8.1. Chart K_3

We obtain the vector field in chart K_3 by inserting condition (50a) into the fast problem (49). This vector field is de-singularized at $w_3 = 0$ by division of e^{1/w_3} . For the sake of readability we drop the subscripts:



$$\begin{aligned}
 \dot{w} &= we^{-\frac{2}{w}} \left(y + \frac{x+1}{\xi} \right), \\
 \dot{x} &= -\varepsilon(x+1+\alpha) + xe^{-\frac{2}{w}} \left(y + \frac{x+1}{\xi} \right), \\
 \dot{y} &= \varepsilon w(1 - e^{-\frac{1}{w}}) + ye^{-\frac{2}{w}} \left(2y + \frac{x+1}{\xi} \right), \\
 \dot{\varepsilon} &= 0.
 \end{aligned} \tag{59}$$

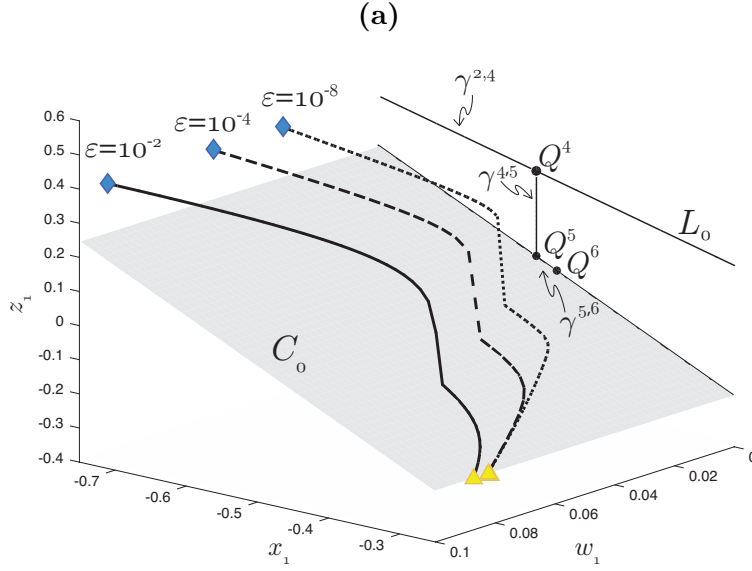


Figure 11: Figure (a): numerical simulation of (1) for $\varepsilon \in \{10^{-8}, 10^{-4}, 10^{-2}\}$, $\alpha = 0.9$ and $\xi = 0.5$. In (b): portion of Γ_ε visible in chart K_3 , i.e. between the green lower triangle and the red square. In (a): portion of Γ_ε visible in K_1 , i.e. between the blue diamond and the yellow upper triangle. We remark that the portion between the blue triangle and the red square is visible both in K_3 and K_1 since the two charts overlap for $y_3 > 0$ or $z_1 > 0$. Colours are available in the online version.

System (59) is a four-dimensional vector field defined on \mathbb{R}^4 where we treat ε as a variable. The set $w = \varepsilon = 0$ consists of non-hyperbolic fixed points of (59) and the two lines $C_{0,\infty}$ and L_0 (54) are contained within this set. Since we consider a regime of w sufficiently small, we approximate $1 - e^{-1/w} \simeq 1$ in the y -equation of (59) to simplify the computations. Qualitatively this has no effects on the results.

We blow-up (59) around Q^1 in order to extend the hyperbolicity of C_0 up to infinity. To do so we need to get rid of the exponential terms. We deal with it by introducing a new variable q :

$$q = e^{-\frac{2}{w}}, \quad (60)$$

so that the extended system contains only algebraic terms in its variables (Kristiansen 2016). Indeed by differentiating (60) with respect to time we obtain:

$$\begin{aligned}\dot{q} &= 2w^{-2}\dot{w}e^{-\frac{2}{w}}, \\ &= 2w^{-1}q\left(y + \frac{x+1}{\xi}\right),\end{aligned}\tag{61}$$

where we have used (59) and (60). Inserting (61) into (59) we obtain the five-dimensional vector field:

$$\begin{aligned}\dot{w} &= w^2q\left(y + \frac{x+1}{\xi}\right), \\ \dot{x} &= -\varepsilon w(x+1+\alpha) + xqw\left(y + \frac{x+1}{\xi}\right), \\ \dot{y} &= \varepsilon w^2 + yqw\left(y + \frac{x+1}{\xi}\right), \\ \dot{q} &= 2q^2\left(y + \frac{x+1}{\xi}\right), \\ \dot{\varepsilon} &= 0.\end{aligned}\tag{62}$$

after multiplying the right hand side by w . The evolution of q in (62) is slaved by w through (60). However, this dependence is not explicit and we will refer to it only when needed. We refer to (Kristiansen 2016) for further details on this approach. System (62) has a 3-dimensional space of non-hyperbolic fixed points for $\varepsilon = q = 0$, since each point has a quintuple zero eigenvalue. To overcome the degeneracy we introduce the blow-up map:

$$q = \bar{r}\bar{q}, \quad \varepsilon = \bar{r}\bar{\varepsilon},\tag{63}$$

with $(\bar{q}, \bar{\varepsilon}) \in S^1$ and $\bar{r} \geq 0$ while the variables $(w, x, y) \in \mathbb{R}^3$ in (62) are kept unchanged. We remark that the quantity ε in (63) is a constant, hence the blown-up space is foliated by invariant hyperboloids. We study the two local charts:

$$\mathcal{K}_1 : \quad q = r_1, \quad \varepsilon = r_1\varepsilon_1,\tag{64a}$$

$$\mathcal{K}_2 : \quad q = r_2q_2, \quad \varepsilon = r_2.\tag{64b}$$

Notice that $q_2 = O(1)$ in chart \mathcal{K}_2 corresponds to $w = O(\ln^{-1} \varepsilon^{-1})$ or $z_2 = O(\ln \varepsilon^{-1})$ through (60). This is the relevant regime for the naïve identification of L_0 as in (9).

Chart \mathcal{K}_1 To simplify the analysis we place the x -axis of (62) on C_0 by introducing the new coordinate $\tilde{x} = x + \xi y + 1$ so that Q^1 is now in the origin of chart \mathcal{K}_3 . We insert (64a) into (62) and divide out a common factor of r_1 to obtain the desingularized system in chart \mathcal{K}_1 . This system is independent of r_1 therefore we restrict the analysis to the remaining four variables $(w, \tilde{x}, y, \epsilon_1)$ and we drop the subscript. The origin of the reduced system is still degenerate with all zero eigenvalues. To overcome the degeneracy we introduce the following blow-up of $C_{0,\infty}$:

$$w = \bar{r}\bar{w}, \quad \tilde{x} = \bar{r}\bar{\tilde{x}}, \quad \epsilon = \bar{r}\bar{\epsilon},$$

where $(\bar{w}, \bar{\tilde{x}}, \bar{\epsilon}) \in S^2$ and $\bar{r} \geq 0$ small, while the variable $y \in \mathbb{R}$ is kept unchanged. We study charts \mathcal{K}_1 and \mathcal{K}_2 that are defined for $\bar{w} = 1$ and $\bar{\epsilon} = 1$ respectively. Chart \mathcal{K}_1 has an attracting 3-dimensional center manifold M_1 in the origin. This manifold is the extension of the slow-manifold S_ε (see Proposition 6.1) into chart \mathcal{K}_1 when $\varepsilon = \text{const.}$ and $q = e^{-2/w}$. Thus we can extend the hyperbolicity of C_0 up to $C_{0,\infty}$ for $\bar{\epsilon} = 0$ and recover the contraction to Q^1 of Figure 6(c). We follow the unique unstable direction of Q^1 that sits on the sphere $\bar{r} = 0$. This direction exits chart \mathcal{K}_1 for $\bar{\epsilon}$ large and contracts to the origin of chart \mathcal{K}_2 along the invariant plane $\bar{r} = 0$. Using hyperbolic methods we follow the unique 1-dimensional unstable manifold γ_2^1 departing from the origin of chart \mathcal{K}_2 into chart \mathcal{K}_2 , where it enters with q_2 small.

Chart \mathcal{K}_2 We substitute (64b) into (62) and divide the right-hand side by r_2 to obtain the dynamics in chart \mathcal{K}_2 . The system is independent of r_2 and we restrict the analysis to (w, x, y, q_2) . The unstable manifold $\gamma_2^1 := \{(w, x, y, q_2) \in \mathcal{K}_2 \mid (w, x, y) = (0, -1, 0), q_2 \geq 0\}$ contracts towards the fixed point:

$$(w, x, y, q_2) = (0, -1, 0, 0). \tag{65}$$

The point (65) belongs to a plane of non-hyperbolic fixed points with $w = q_2 = 0$ and to overcome the loss of hyperbolicity we introduce the blow-up map (after having dropped the subscript):

$$w = \bar{r}\bar{w}, \quad q = \bar{r}\bar{q}, \tag{66}$$

where $(\bar{w}, \bar{q}) \in S^1$ and $\bar{r} \geq 0$. We study charts $\hat{\mathcal{K}}_1$ and $\hat{\mathcal{K}}_2$ that are defined for $\bar{w} = 1$ and $\bar{q} = 1$ respectively.

Chart \hat{K}_1 We insert (66) with $\bar{w} = 1$ into the vector field of chart \mathcal{K}_2 and drop the bar. We divide the system by r to obtain the de-singularized equations:

$$\begin{aligned} \dot{r} &= r^2 q \left(y + \frac{x+1}{\xi} \right), \\ \dot{x} &= -(x+1+\alpha) + xrq \left(y + \frac{x+1}{\xi} \right), \\ \dot{y} &= r + yrq \left(y + \frac{x+1}{\xi} \right), \\ \dot{q} &= q^2(2-r) \left(y + \frac{x+1}{\xi} \right). \end{aligned} \tag{67}$$

In the following important lemma we identify the line L_0 and the segment $\gamma^{1,2}$:

Lemma 8.1 *In chart \hat{K}_1 there exists an attracting 3-dimensional center manifold:*

$$x = -1 - \alpha + O(r+q), \tag{68}$$

whose intersection with the plane $r = q = 0$ corresponds to the line L_0 (54a). The trajectory $\gamma^{1,2}$ defined in (55) connects along a stable fiber the point (65) to Q^2 (53a).

Proof (67) has a line of fixed points for $r = q = 0, x = -1 - \alpha, y \in \mathbb{R}$. This line corresponds to L_0 through the coordinate changes (64b), (66). The linearized dynamics on L_0 is hyperbolic only in the x -direction and furthermore is stable. Therefore (68) appears for r, q sufficiently small. The point (65) in chart \hat{K}_1 becomes:

$$(r, x, y, q) = (0, -1, 0, 0), \tag{69}$$

hence there is a solution backwards asymptotic to (69) and forward asymptotic to $Q^2 \in L_0$ (recall (53a)) through a stable fiber. This connection corresponds to $\gamma^{1,2}$. \square

We insert (68) into (67) to obtain the dynamics on the center manifold. The resulting vector field has a line of non-hyperbolic fixed points, corresponding to L_0 , for $r = q = 0$ since each point has a triple zero eigenvalue. We gain hyperbolicity of this line by introducing the blow-up map:

$$r = \rho\sigma, \quad q = \rho, \tag{70}$$

where $\rho \geq 0, \sigma \geq 0$. In chart (70) the point Q^2 (53a) is blown-up to the σ -axis $\{y = \rho = 0, \sigma \geq 0\}$. Similarly Q^4 (53b) corresponds to the line $\{y = 2\alpha/\xi, \rho = 0, \sigma \geq 0\}$. We divide the vector field of chart (70) by the common divisor ρ and obtain:

$$\begin{aligned}\dot{\sigma} &= \sigma(-2 + \rho\sigma + \rho^2) \left(y - \frac{\alpha}{\xi} \right) (1 + \mathcal{O}(\rho)), \\ \dot{y} &= \sigma + y\rho\sigma \left(y - \frac{\alpha}{\xi} \right) (1 + \mathcal{O}(\rho)), \\ \dot{\rho} &= \rho(2 - \rho\sigma) \left(y - \frac{\alpha}{\xi} \right) (1 + \mathcal{O}(\rho)).\end{aligned}\tag{71}$$

Following equations (65) and γ_2^1 we enter chart (70) with $\sigma = 0$ and $y = 0$. Subsequently, by following $\gamma^{1,2}$ we have $\rho = 0$. In the following we describe the dynamics within L_0 and identify $\gamma^{2,4}$ as a heteroclinic orbit.

Lemma 8.2 *System (71) has two invariant planes for $\rho = 0$ and $\sigma = 0$. Their intersection $\rho = \sigma = 0$ is a line of fixed points. We have:*

- *The origin $(\sigma, y, \rho) = (0, 0, 0)$ has a strong stable manifold:*

$$W^s(0, 0, 0) := \{(\sigma, y, \rho) \in \mathbb{R}^2 \times \mathbb{R}_+ \mid \sigma = 0, y = 0, \rho \geq 0\}.\tag{72}$$

- *There exists a heteroclinic connection:*

$$\gamma^{2,4} = \left\{ (\sigma, y, \rho) \in \mathbb{R}^2 \times \mathbb{R}_+ \mid \sigma = 2\frac{\alpha}{\xi}y - y^2, y \in (0, 2\alpha/\xi), \rho = 0 \right\}.\tag{73}$$

joining $(\sigma, y, \rho) = (0, 0, 0)$ backwards in time with $(\sigma, y, \rho) = (0, 2\alpha/\xi, 0)$ forward in time.

- *The point $(\sigma, y, \rho) = (0, 2\alpha/\xi, 0)$ has a strong unstable manifold:*

$$W^u(0, 2\alpha/\xi, 0) := \{(\sigma, y, \rho) \in \mathbb{R}^2 \times \mathbb{R}_+ \mid \sigma = 0, y = 2\alpha/\xi, \rho \geq 0\}.\tag{74}$$

The results of Lemma 8.2 are summarized in Figure 12.

Remark 8 *Upon blowing down, the expression in (73) gives $\gamma^{2,4}$ in (56). We use the same symbol in (73) and (56) for simplicity.*

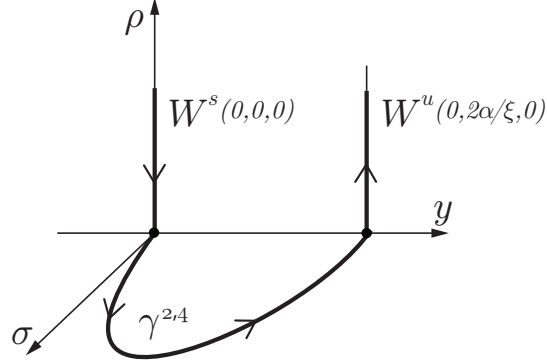


Figure 12: Dynamics in chart \hat{K}_1 . The plane $\rho = 0$ corresponds to the blown-up line L_0 . Here the singular dynamics contracts to L_0 and then is expelled from it.

Proof On the invariant plane $\sigma = 0$ we have the following dynamics:

$$\begin{aligned} \dot{y} &= 0, \\ \dot{\rho} &= 2\rho \left(y - \frac{\alpha}{\xi} \right) (1 + O(\rho)). \end{aligned} \tag{75}$$

This plane is foliated with invariant lines in the y -direction. The solution of (75) with $y = 0$ is (72) and contracts towards the invariant plane $\rho = 0$. Hence this trajectory acts as a strong stable manifold. We substitute $\rho = 0$ into (71) and after dividing by σ we obtain the explicit solution (73) given the initial condition in the origin. This solution is forward asymptotic to $(\sigma, y, \rho) = (0, 2\alpha/\xi, 0)$. Eventually ρ expands on the strong unstable manifold (74), that is the solution of (75) with $y = 2\alpha/\xi$. \square

Using hyperbolic methods we follow the unstable manifold $W^u(0, 2\alpha/\xi, 0)$ into chart \hat{K}_2 where it contracts towards the origin along the invariant plane $\bar{r} = 0$. We continue this trajectory by following the unstable manifold of the origin on the plane $\bar{w} = 0$. We continue this manifold into chart \mathcal{K}_1 , since eventually chart \mathcal{K}_2 is no longer suited to describe this trajectory. Here the variable ϵ decreases exponentially and for $\epsilon = w = 0$ we obtain a layer problem. Therefore from Q^4 we follow after desingularization a fast fiber $\gamma^{4,5}$ that corresponds to the solution of this layer problem and that contracts to the point Q^5 on C_0 . Since Q^5 may not be visible in chart K_3 , we compute its coordinates in chart K_1 .

8.2. Chart K_1

We insert (51b) into the fast problem (49) and divide by e^{z_1/w_1} to obtain the desingularized vector field in chart K_1 . We drop the subscript henceforth for the sake of readability:

$$\begin{aligned} \dot{w} &= -\varepsilon w^2(1 - e^{-z/w}), \\ \dot{x} &= -\varepsilon(x + (1 + \alpha)z) - \varepsilon x w(1 - e^{-z/w}), \\ \dot{z} &= -e^{-2z/w} \left(1 + \frac{x + z}{\xi}\right) - \varepsilon z w(1 - e^{-z/w}). \end{aligned} \tag{76}$$

In chart K_1 the layer problem is obtained by requiring $\varepsilon = 0$ in (76). Hence the dynamics on the layer problem is only in the z -direction and the fibers are all vertical. In particular the fiber $\gamma^{4,5}$ is written as in (57) since it departs from $K_{31}(Q^4)$. It follows that $\gamma^{4,5}$ is forward asymptotic to the point Q^5 defined in (53c). The point Q^5 is connected to Q^6 through the segment $\gamma^{5,6}$, according to the analysis of the reduced problem of section 5. From the point Q^6 the solution is connected to the point Q^1 through the manifold $W^{c,u}$. This closes the singular cycle Γ_0 .

Figure 10(c) illustrates the dynamics in chart K_1 . We remark that the change of coordinates from chart K_3 to chart K_1 is defined for $z_1 > 0$ and therefore when $\alpha > 1$ the point Q^5 is visible only in chart K_1 .

9. Outline of a proof

To prove Conjecture 7.1 we would have to consider a section $\Lambda_1 := \{w_1 = \delta\}$ transverse to $W^{c,u}$ where $\delta > 0$ is small but fixed. Using the blow-up in chart K_3 we can track a full neighbourhood $N \subset \Lambda_1$ of $\Lambda_1 \cap W^{c,u}$ using Proposition 5.2, $\gamma^{1,2}, \gamma^{2,4}, \gamma^{4,5}, \gamma^{5,6}$ and $W^{c,u}$ respectively, to obtain a return map $P_1 : N \rightarrow N$ for ε sufficiently small. For $\varepsilon = 0$ the forward flow of N contracts to the point Q^1 . This would provide the desired contraction of P_1 and establish, by the contraction mapping theorem, the existence of the limit cycle Γ_ε satisfying $\Gamma_\varepsilon \rightarrow \Gamma_0$ for $\varepsilon \rightarrow 0$.

10. Conclusions

We have considered the one dimensional spring-block model that describes the earthquake faulting phenomenon. We have used geometric singular perturbation theory and the blow-up method to provide a detailed description of the periodicity of the

earthquake episodes, in particular we have untangled the increase in amplitude of the cycles for $\varepsilon \rightarrow 0$ and their relaxation oscillation structure. We have shown that the limit cycles arise from a degenerate Hopf bifurcation. The degeneracy is due to an underlying Hamiltonian structure that leads to large amplitude oscillations. Using the Poincaré compactification together with the blow-up method, we have described how these limit cycles behave near infinity in the limit of $\varepsilon \rightarrow 0$. A full detailed proof of Conjecture 7.1, including the required careful estimation of the contraction, will be the subject of a separate manuscript.

We have observed that the notation of quasi-static slip motion to define the reduced problem (11) is misleading. Indeed the solutions of (11) have an intrinsic slow-fast structure resembling the stick-slip oscillations. Our analysis also shows that the periodic solutions of (1) cannot be investigated by studying the so-called quasi-static slip phase and the stick-slip phase separately, as it is done in (Ruina 1983, Gu et al. 1984), since the two phases are connected by the non-linear terms of (1). We also suggest suitable coordinate sets and time rescales to deal with the stiffness of (1) during numerical simulations. We hope that a deeper understanding of the structure of the earthquake cycles may be of help to the temporal predictability of the earthquake episodes.

We presuppose that we can apply some of the ideas in this manuscript to the study of the 1-dimensional spring-block model with Dieterich state law. Indeed in this new system the fixed point in the origin behaves like a saddle, the critical manifold loses hyperbolicity like (8) and solutions reach infinity in finite time for $\varepsilon \rightarrow 0$. Moreover we think that these ideas can also be used to study the continuum formulation of the Burridge and Knopoff model with Ruina state law, in particular to analyse the self-healing slip pulse solutions (Heaton 1990). Indeed this latter model has the same difficulties of (1) in terms of small parameter and non-linearities of the vector field (Erickson et al. 2011). We remark that the self-healing slip pulse solutions are considered to be related to the energy of an earthquake rupture.

Acknowledgments

The first author thanks Thibault Putelat and Björn Birnir for the useful discussions. We acknowledge the Idella Foundation for supporting the research. This research was partially done whilst the first author was a visiting Researcher at the Centre de

Recerca Matemàtica in the Intensive Research Program on Advances in Nonsmooth Dynamics.

References

- Belardinelli M E & Belardinelli E 1996 *Nonlinear Processes in Geophysics* **3**(3), 143–149.
- Ben-Zion Y 2008 *Reviews of Geophysics* **46**(4). RG4006.
- Bizzarri A 2010 *Geophysical Research Letters* **37**(20). L20315.
- Bossolini E, Brøns M & Kristiansen K U 2016 *ArXiv e-prints arXiv:1603.02448v1 [math.DS]* .
- Burridge R & Knopoff L 1967 *Bulletin of the Seismological Society of America* **57**(3), 341–371.
- Carlson J M & Langer J S 1989 *Physical Review A* **40**(11), 6470–6484.
- Carlson J M, Langer J S, Shaw B E & Tang C 1991 *Physical Review A* **44**(2), 884–897.
- Chicone C 2006 *Ordinary differential equations with applications* Springer Science+Business Media.
- Chow S N, Li C & Wang D 1994 *Normal Forms and Bifurcation of Planar Vector Fields* Cambridge University Press.
- Corless R M, Gonnet G H, Hare D E G, Jeffrey D J & Knuth D E 1996 *Advances in Computational Mathematics* **5**(1), 329–359.
- Dieterich J H 1972 *Journal of Geophysical Research* **77**(20), 3690–3697.
- Dieterich J H 1978 *Pure and Applied Geophysics* **116**(4-5), 790–806.
- Dieterich J H 1979 *Journal of Geophysical Research* **84**(B5), 2161–2168.
- Dumortier F & Roussarie R 1996 *Memoirs of the American Mathematical Society* **121**(577).
- Eckhaus W 1973 *Matched asymptotic expansions and singular perturbations* North-Holland Publ.
- Erickson B, Birnir B & Lavallée D 2008 *Nonlinear Processes in Geophysics* **15**(1), 1–12.
- Erickson B, Birnir B & Lavallée D 2011 *Geophysical Journal International* **187**(1), 178–198.
- Fan Q, Xu C, Niu J, Jiang G & Liu Y 2014 *Journal of Seismology* **18**(3), 637–649.
- Fenichel N 1974 *Indiana University Mathematics Journal* **23**(12), 1109–1137.
- Fenichel N 1979 *Journal of Differential Equations* **31**(1), 53–98.
- Gu J C, Rice J R, Ruina A L & Tse S T 1984 *Journal of the Mechanics and Physics of Solids* **32**(3), 167–196.
- Gucwa I & Szmolyan P 2009 *Discrete and Continuous Dynamical Systems - Series S* **2**(4), 783–806.
- Heaton T H 1990 *Physics of the Earth and Planetary Interiors* **64**(1), 1–20.
- Jones C K R T 1995 in R Johnson, ed., ‘Dynamical Systems’ Vol. 1609 of *Lecture Notes in Mathematics* Springer Berlin Heidelberg pp. 44–118.
- Kaper T J 1999 in ‘Proceedings of Symposia in Applied Mathematics’ Vol. 56 American Mathematical Society pp. 85–132.
- Kristiansen K U 2016 *ArXiv e-prints arXiv:1603.01821 [math.DS]* .
- Krupa M & Szmolyan P 2001 *SIAM Journal on Mathematical Analysis* **33**(2), 286–314.
- Kuehn C 2014 *Nonlinearity* **27**(6), 1351–1366.
- Kuehn C 2015 *Multiple Time Scale Dynamics* Vol. 191 of *Applied Mathematical Sciences* Springer International Publishing.
- Lapusta N, Rice J R, Ben-Zion Y & Zheng G T 2000 *Journal of Geophysical Research* **105**(B10), 23765–23789.

- Madariaga R 1998 Complex Heterogeneous Faulting Models. Unpublished notes (Preprint).
- Madariaga R & Cochard A 1996 *Proceedings of the National Academy of Sciences of the United States of America* **93**(9), 3819–3824.
- Marone C 1998a *Nature* **391**(6662), 69–72.
- Marone C 1998b *Annual Review of Earth and Planetary Sciences* **26**, 643–696.
- Marone C, Vidale J E & Ellsworth W L 1995 *Geophysical Research Letters* **22**(22), 3095–3098.
- Nadeau R M & McEvilly T V 1999 *Science* **285**(5428), 718–721.
- Nakatani M 2001 *Journal of Geophysical Research: Solid Earth* **106**(B7), 13347–13380.
- Pomeau Y & Berre M L 2011 *ArXiv e-prints arXiv:1107.3331 [physics.geo-ph]* .
- Putelat T, Willis J R & Dawes J H P 2008 *Philosophical Magazine* **88**(28–29), 3219–3243.
- Ranjith K & Rice J R 1999 *Journal of the Mechanics and Physics of Solids* **47**(6), 1207–1218.
- Rankin J, Desroches M, Krauskopf B & Lowenberg M 2011 *Nonlinear Dynamics* **66**(4), 681–688.
- Rice J R & Ruina A L 1983 *Journal of Applied Mechanics* **50**(2), 343–349.
- Rice J R & Tse S T 1986 *Journal of Geophysical Research* **91**(B1), 521–530.
- Ruina A 1983 *Journal of Geophysical Research: Solid Earth* **88**(B12), 10359–10370.
- Vidale J E, Ellsworth W L, Cole A & Marone C 1994 *Nature* **368**(6472), 624–626.
- Zechar J D & Nadeau R M 2012 *Geophysical Journal International* **190**(1), 457–462.